

# Bounded asymptotics for high-order moments in wall turbulence

Xi Chen

Key Laboratory of Fluid Mechanics of Ministry of Education,  
Beihang University (Beijing University of Aeronautics and Astronautics), Beijing 100191, PR China \*

Katepalli R. Sreenivasan

Tandon School of Engineering, Courant Institute of Mathematical Sciences,  
and Department of Physics, New York University, New York 10012, USA †

(Dated: June 28, 2024)

Turbulent wall-flows are the most important means for understanding the effects of boundary conditions and fluid viscosity on turbulent fluctuations. There has been considerable recent research on mean-square fluctuations. Here, we present expressions for high-order moments of streamwise velocity fluctuation  $u$ , in the form  $\langle u^{+2q} \rangle^{1/q} = \alpha_q - \beta_q y^{*1/4}$ ;  $q$  is an integer,  $\alpha_q$  and  $\beta_q$  are constants independent of the friction Reynolds number  $Re_\tau$ , and  $y^* = y/\delta$  is the distance away from the wall, normalized by the flow thickness  $\delta$ ; in particular,  $\alpha_q = \mu + \sigma q$  according to the ‘linear  $q$ -norm Gaussian’ process, where  $\mu$  and  $\sigma$  are flow-independent constants. Excellent agreement is found between these formulae and available data in pipes, channels and boundary layers for  $1 \leq q \leq 5$ . For fixed  $y^+ = y^* Re_\tau$ , the present formulation leads to the bounded state  $\langle u^{+2q} \rangle^{1/q} = \alpha_q$  as  $Re_\tau \rightarrow \infty$  while the attached eddy model predicts that the moments continually grow as log Reynolds number.

*Introduction:* For over a century, a vexing problem in turbulence research has been how turbulence fluctuations vary near a smooth solid wall; see [1]. The classical paradigm is that, when scaled by the so-called friction velocity  $u_\tau \equiv \sqrt{\tau_w/\rho}$ , where  $\tau_w$  is the shear stress at the wall and  $\rho$  the fluid density, various averages of turbulence fluctuations are invariant with respect to the Reynolds number  $Re_\tau (\equiv u_\tau \delta/\nu)$ , where  $\delta$  is the thickness of the turbulent boundary layer (TBL), pipe radius or channel half-height, and  $\nu$  is the fluid viscosity). However, data accumulated in the last two decades from laboratory experiments [2–6] as well as direct numerical simulations (DNS) [7–13] show that the mean square fluctuations keep increasing in the known Reynolds number range. A prevailing result, based on the so-called attached eddy model originating with [14], is that this increase persists indefinitely as  $\ln Re_\tau$  (see [15–17] and references therein). Quite a different result [18–20], based on the so-called bounded dissipation model (see also [21]), is that the observed increase is a finite- $Re_\tau$  effect, which vanishes as  $Re_\tau \rightarrow \infty$ .

The theoretical underpinnings of both results are not fool-proof (see below for more comments), so reliance has to be placed on the agreement with empirical results while deciding the relative merits of the models. Comparison of low-order moments in the available data range is ambiguous in some instances—though an independent assessment [22], besides our own [18–20], documents support for the bounded law over the attached eddy results—so a detailed consideration of high-order moments is essential. Here, we consider the wall-normal profiles of high-order velocity fluctuation moments, make detailed data comparisons for the two formulations and provide a few general conclusions. This is the purpose of this Letter.

*Theoretical considerations:* According to attached eddy model, the variance of streamwise velocity  $u$  follows a logarithmic decay in the flow region beyond the near wall peak, i.e.,

$$\langle u^{+2} \rangle = B_1 - A_1 \ln(y^*), \quad (1)$$

which has been generalized in [23] for high-order moments as

$$\langle u^{+2q} \rangle^{1/q} = B_q - A_q \ln(y^*). \quad (2)$$

Here, the superscript  $+$  indicates normalization by  $u_\tau$  and  $y^* = y/\delta$ . The brackets  $\langle \rangle$  indicate temporal averages; and  $A_q$  and  $B_q$  are constants independent of  $y^*$  and  $Re_\tau$  but depend on the moment order  $q$ .

Equation (1) builds on the idea of turbulent eddies effectively attached to the wall, with their number density varying inversely with  $y^*$  [16]. Because the identification of a clear eddy structure is fraught with uncertainties [25], the  $k^{-1}$  velocity spectrum [26] is sometimes thought to be another possible rationale for the same idea; but that, too, has not been observed unambiguously [27, 28]. In going from (1) to (2), a Gaussian distribution of  $u$  is assumed, which leads to  $\langle u^{+2q} \rangle^{1/q} = [(2q-1)!!]^{1/q} \langle u^{+2} \rangle^{1/2}$  with  $q!! \equiv q(q-2)(q-4)\dots 1$ , but the slopes  $A_q$  depart significantly from the Gaussian prediction [23].

The alternative boundedness proposal is

$$\langle u^{+2q} \rangle^{1/q} = \alpha_q - \beta_q (y^*)^{1/4}, \quad (3)$$

where  $\alpha_q$  and  $\beta_q$  are constants independent of  $y^*$  and  $Re_\tau$ . For reference the variance of  $u$  for  $q = 1$  in (3) is

$$\langle u^{+2} \rangle = \alpha_1 - \beta_1 (y^*)^{1/4}. \quad (4)$$

The procedure for deriving (4) is summarized here, with details to be found in [20], where a preliminary comparison with data was made. We have an inner expansion

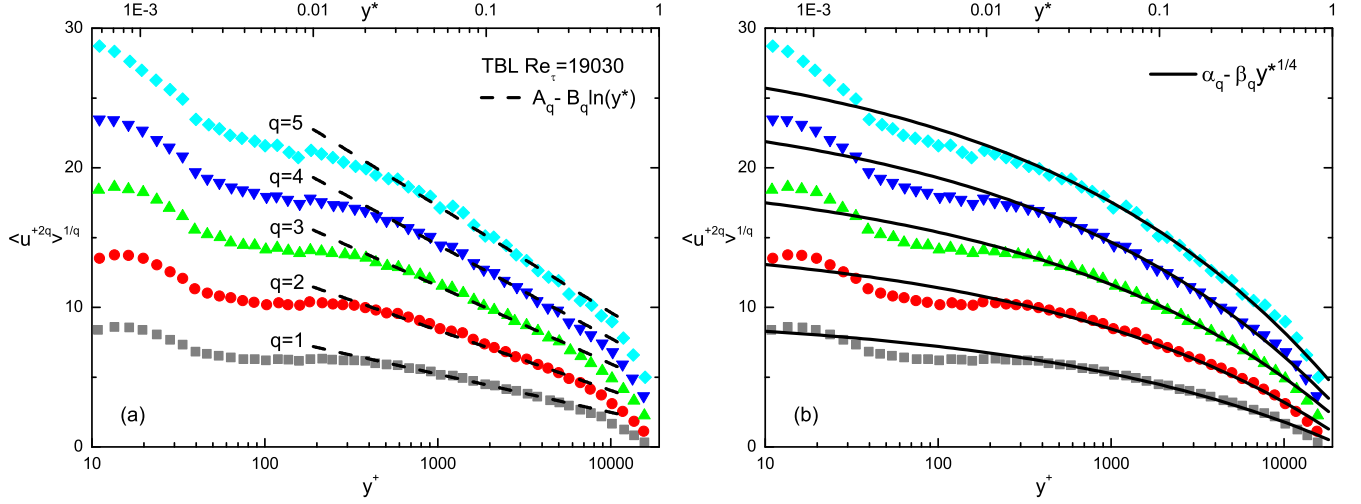


FIG. 1. Wall-normal variation of  $\langle u^{+2q} \rangle^{1/q}$  for  $q = 1 - 5$  in TBL compared with (a) the logarithmic decay of the attached eddy model in Eq. (2) by Meneveau & Marusic [23] (dashed lines), and (b) the bounded dissipation result given by (3) (solid lines);  $q$  values are the same as in (a). In both panels, the bottom abscissa is in viscous unit  $y^+ = y^*/Re_\tau$ , and the top in the outer unit  $y^* = y^+/Re_\tau$ . Symbols are data measured by Hutchins *et al.* [24].

$\langle u^{+2} \rangle = f_0(y^+) + f_1(y^+)g(Re_\tau)$ , and an outer expansion  $\langle u^{+2} \rangle = F_0(y^*)$ . Here,  $y^+ = y^*Re_\tau$  is the inner viscous scale, and the Gauge function  $g(Re_\tau) = Re_\tau^{-1/4}$  depicts the finite  $Re_\tau$  dependence, determined via a consideration of the influence of the outer Kolmogorov scales [18]. The matching between the two expansions results in (4). Equation (3) could be regarded as a generalization of (4) by replacing  $\langle u^{+2} \rangle$  by  $\langle u^{+2q} \rangle^{1/q}$ . Another way to derive (3) is to invoke a ‘linear- $q$ -norm Gaussian’ (LQNG) process developed in [19], which is different from the derivation of (2) from the Gaussian assumption, as will be explained subsequently.

*Comparison with experiments:* Below, a side-by-side comparison of (2) and (3) with data will be presented, and variations of  $\alpha_q$  and  $A_q$  will be examined for understanding their underlying stochastic properties in the asymptotic limit of  $Re_\tau \rightarrow \infty$ .

Reminiscent of the standard overlap in the form of the well-known log-law, the generalized form (2) was proposed in [23] for an intermediate region approximately in the range  $400 < y^+ < 0.3Re_\tau$ . For a decade of  $y^+$  in this intermediate region, an  $Re_\tau > 13,000$  is required (see also [22]), which is larger than that available from DNS. We thus start with comparisons for high- $Re_\tau$  experiments of TBL and pipe flows, and then consider the DNS data for channels obtained at more moderate  $Re_\tau$ . The data uncertainty is not addressed here as it has been discussed in the original references.

Specifically, Fig. 1 shows  $\langle u^{+2q} \rangle^{1/q}$  of TBL at  $Re_\tau \approx 19,000$  for  $q = 1 - 5$ , measured by Hutchins *et al.* [24] in the Melbourne wind tunnel. This dataset is the one used in [23] to illustrate the generalized representation (2).

Shown by dashed lines in Fig. 1a are the best fits given by (2); there is a decent agreement with the data in an intermediate  $y^+$  range, with the best fits for  $(A_q, B_q)$  given by: (1.19, 1.71), (2.06, 2.50), (2.93, 3.23), (3.81, 4.12), and (4.68, 5.03) for  $q = 1 - 5$ , respectively. The fitted value  $A_1 = 1.19$  differs from the earlier value of  $A_1 = 1.25$  by 5%, which is within uncertainty [23]. The intercepts  $B_q$  increase with increasing  $q$ , but a closer look at Fig. 1a reveals that the inner limits for the fits (2) begin increasingly farther away from the wall—for example,  $y^+ \approx 200$  for  $q = 1$  compared to  $y^+ \approx 400$  for  $q = 5$ . The standard logarithmic region will be continually eroded if this trend continues. We should also note that the fit becomes more of a tangent to the data for larger  $q$ .

On the other hand, the bounded behavior (3) reproduces data better in a wide flow domain (Fig. 1b), i.e. from  $y^+ = 200$  to almost the edge of the boundary layer. The best fits for  $(\alpha_q, \beta_q)$  are: (9.7, 9.3), (15.2, 14.1), (20.2, 17.9), (25.2, 22), (29.5, 25) for  $q = 1 - 5$ , respectively. Two further points may be noted. First, since  $\langle u^{+2q} \rangle^{1/q}$  remains positive for  $y^* = 1$ ,  $\beta_q$  is by necessity slightly smaller than  $\alpha_q$ . Second,  $\langle u^{+2q} \rangle^{1/q} = \alpha_q$  is the asymptotic plateau for  $y^* \rightarrow 0$ , which can therefore be used to approximate the inner profile. For example, closer to the wall within the so-called buffer layer, (3) fits the data approximately. Indeed, the deviation from data is  $O(1)$  for the entire flow domain. However, this is not the case for the attached eddy model [15] for which the peak scales as  $(A_q/2) \ln Re_\tau$ , whereas the near wall extension of (2) suggests a magnitude  $A_q \ln Re_\tau$ ; the difference between the two is of order  $\ln Re_\tau$  which diverges as  $Re_\tau \rightarrow \infty$ . Hence, one cannot simply extrapolate (2)

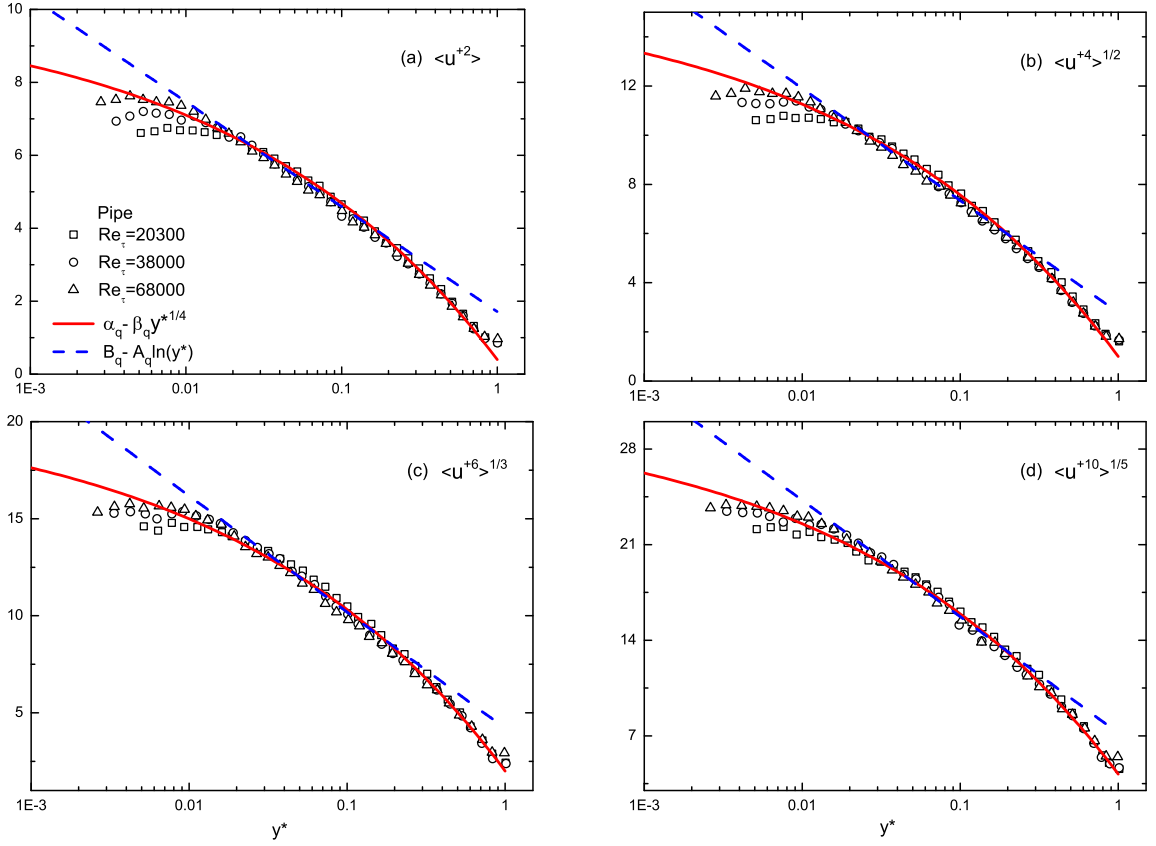


FIG. 2. Wall-normal variations of  $\langle u^{+2p} \rangle^{1/p}$  in pipes for (a)  $p = 1$ ; (b)  $p = 2$ ; (c)  $p = 3$  and (d)  $p = 5$ . Solid lines (red) are the bounded-decay formula in (3), whilst dashed lines (blue) are the log-decay in (2). Symbols are experimental data from Hultmark *et al* [29].

to approximate the near wall profile.

Moving on to the pipe flow Figs. 2a-d compare the profiles of  $\langle u^{+2p} \rangle^{1/p}$  for  $q = 1, 2, 3, 5$  with data measured by Hultmark *et al.* [29] in the Princeton Superpipe. Taking data at  $Re_\tau = 20,300$  as the example, the logarithmic fit is obtained in the range  $0.02 < y^* < 0.3$ , which corresponds to the  $400 < y^+ < 0.3Re_\tau$ . For that range, we obtain  $(A_q, B_q)$  as  $(1.25, 1.71)$ ,  $(1.98, 2.78)$ ,  $(2.6, 4.20)$ ,  $(3.7, 7.22)$  for  $q = 1, 2, 3, 5$ , respectively. Again, they appear somewhat like tangents to the data profiles. In comparison, the bounded form agrees closely with data in the whole range  $y^* > 0.02$ , with the best fits of  $(\alpha_q, \beta_q)$  given by  $(10.2, 9.8)$ ,  $(16, 15)$ ,  $(21, 19)$ ,  $(31, 26.8)$  for increasing  $q$ . Note that the same constants produce good data collapse for all other  $Re_\tau$  profiles. To explain, this collapse is the basis for our outer expansion mentioned in the “Theoretical considerations” section. It is clear in Fig. 2 that the bounded form extends almost to the center of pipe, much farther than the log-form ending at  $y^* = 0.3$ . Also, towards the wall, the bounded form characterizes larger segments of the data profiles.

Comparisons with the channel flow are shown in Fig. 3 for the DNS data at  $Re_\tau = 5200$  by Lee & Moser [10].

These high-order moments are obtained from the Johns Hopkins Turbulence Database. More than  $5 \times 10^6$  velocity samples are averaged to obtain these profiles, and the convergence of the probability density function has been checked. As shown in Fig. 3a, the bounded form yields a close representation of data, covering both the near-wall and the center flow regions. For a closer look near the wall, Fig. 3b shows the same plot on the logarithmic abscissa, from which it is clear that the log-form only captures data in a narrow domain (from  $y^+ = 400$  or  $y^* = 0.08$ , to  $y^* = 0.3$ ), while (3) offers a better description for the channel flow as well.

*Asymptotic behaviors:* Different asymptotic behaviors can be deduced for the two proposals. Unlike an unbounded growth of the variance according to (1), a bounded state follows for (4), i.e.,  $\langle u^{+2} \rangle = \alpha_1 \approx 10$  as  $Re_\tau \rightarrow \infty$ . This sharp contrast appears also for higher  $q$ . It is important to understand how  $\alpha_q$  and  $A_q$  vary with  $q$  because they appear in the leading order terms. They are plotted in Fig. 4 for all three flows. For  $A_q$  (normalized by  $A_1$ ), the data vary from one flow to another, with those for channel being the lowest. This is in addition to the sensitivity shown by  $A_1$  with respect

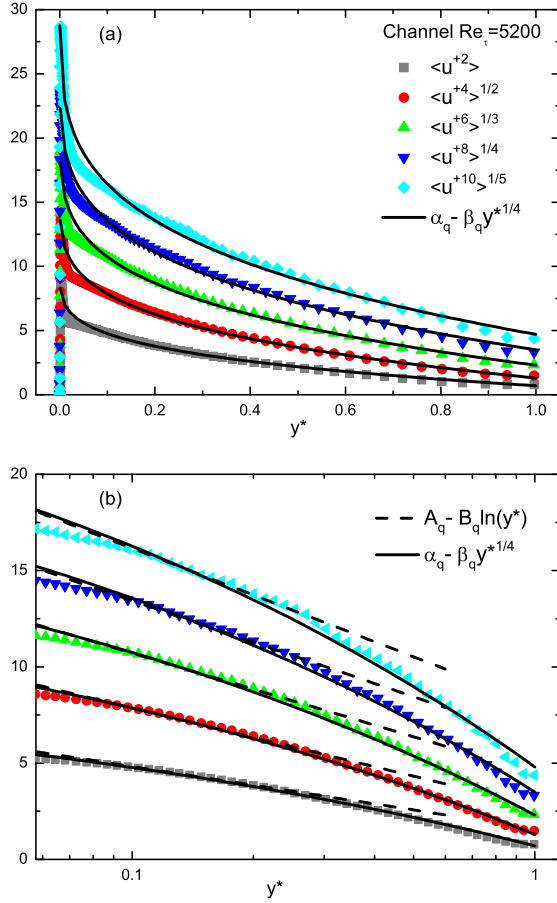


FIG. 3. Wall-normal variation of  $\langle u^{+2q} \rangle^{1/q}$  in the channel for  $q = 1 - 5$ : abscissa in linear scale (a) and in logarithmic scale (b). Symbols are DNS data from Lee & Moser [10]. Solid lines are (3) while dashed lines are (2).

to  $Re_\tau$  [30]. Moreover, following the Gaussian model in [23], one has

$$A_q = A_1[(2q-1)!!]^{1/q}, \quad (5)$$

which is, however, conspicuously higher than the  $A_q$  obtained from Fig. 4a. Such a departure indicates that the Gaussian assumption does not hold and that a different model is needed (e.g., the sub-Gaussian consideration of [31]).

In contrast, the  $\alpha_q$  values for the three flows are quite close to each other and exhibit an excellent linear dependence with the order  $q$  (Fig. 4b). As  $\langle u^{+2q} \rangle^{1/q} = \alpha_q$  for  $y^* \rightarrow 0$ , the linear growth of  $\alpha_q$  corresponds to a LQNG process of  $\phi = (u^+)^2$ , which satisfies the operator reflection symmetry [19] as

$$\mathbf{E} \circ \mathbf{Q}(\phi) = \mathbf{Q} \circ \mathbf{E}(\kappa). \quad (6)$$

Here,  $\kappa = N(\mu, 2\sigma)$  is a Gaussian seed with mean  $\mu$  and variance  $2\sigma$ ;  $\mathbf{E}$  is the operator of exponential transform,

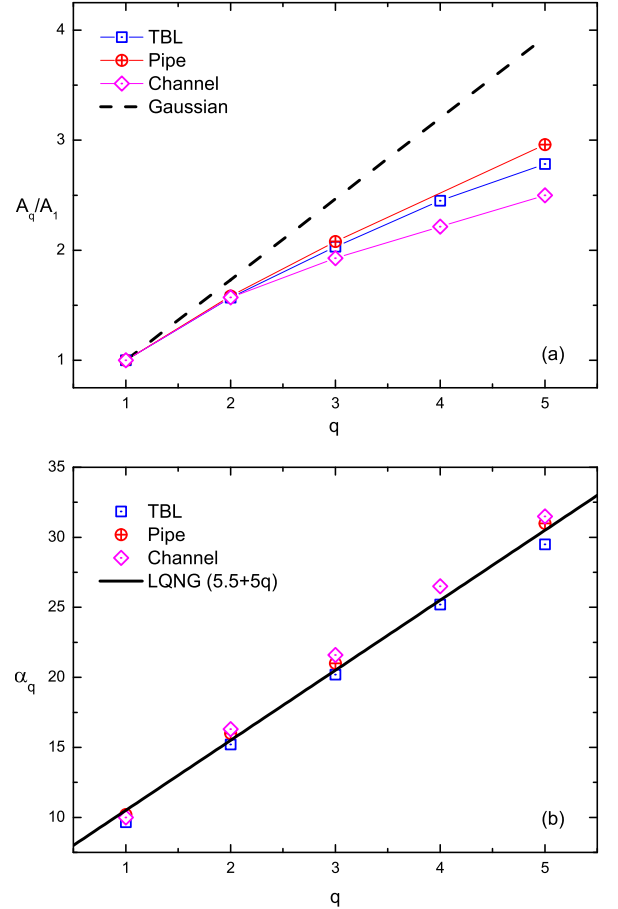


FIG. 4. (a) Ratio of  $A_q/A_1$  varying with order  $q$ ; dashed line represents the Gaussian prediction by (5). (b)  $\alpha_q$  varying with order  $q$ ; solid line indicates the LQNG process in (7).

e.g.  $\mathbf{E}(\kappa) = e^\kappa$ ; and  $\mathbf{Q}$  is the operator of  $q$ -norm estimation, e.g.  $\mathbf{Q}(\phi) = \langle \phi^q \rangle^{1/q}$  with  $\langle \cdot \rangle$  for the expectation. To see the linearity with  $q$ , applying  $\mathbf{E}^{-1}$  (i.e., taking the logarithm) on both sides of (6) yields

$$\begin{aligned} \langle u^{+2q} \rangle^{1/q} = \mathbf{Q}(\phi) &= \mathbf{E}^{-1} \circ \mathbf{Q} \circ \mathbf{E}(\kappa) \\ &= \ln[\langle e^{\kappa q} \rangle^{1/q}] = \mu + \sigma q. \end{aligned} \quad (7)$$

With  $\mu = 5.5$  and  $\sigma = 5$ , (7) thus explains the linear behavior of  $\alpha_q$  in Fig. 4b. Note that the current  $\alpha_q = 5.5 + 5q$  is very close to  $\alpha_q = 5.5 + 5.9q$  from Eq. (4.10) of [19] for the moments inner peak at  $y^+ = 15$ , indicating that the whole flow shares the similar LQNG property.

Finally, we derive (3) from (4) by the LQNG process. According to (6) or (7), the ratio of moments also grows linearly with order, i.e.  $\langle u^{+2q} \rangle^{1/q} / \langle u^{+2} \rangle = (\mu + \sigma q) / (\mu + \sigma) = c_1 + c_2 q$  where  $c_1 = \mu / (\mu + \sigma)$  and  $c_2 = \sigma / (\mu + \sigma)$ . Further with (4) for  $\langle u^{+2} \rangle$ , one obtains (3) for high order moments. The approach is different from the Gaussian hypothesis, but it is evident that LQNG describes Fig. 4b more consistently.

*Conclusions:* In summary, we have shown that the

bounded asymptotic paradigm for high-order moments of wall turbulence shows excellent agreement with data in boundary layers, pipes and channels. The new expression covers a wide range of  $y^+$  and suggests a constant plateau for the moments that grows linearly with the moment order. Future work includes the connection of the present formulation to the flow geometry.

*Acknowledgement.* We are grateful to all the authors cited in figures 1-3 for making their data available. X. Chen appreciates the support by the National Natural Science Foundation of China, No. 12072012 and 11721202, and the “Fundamental Research Funds for the Central Universities”.

---

\* chenxi97@outlook.com

† krs3@nyu.edu

- [1] I. Marusic, B. McKeon, P. Monkewitz, H. Nagib, A. Smits, and K. R. Sreenivasan, *Phys. Fluids* **22**, 065103 (2010).
- [2] M. Hultmark, M. Vallikivi, S. Bailey, and A. Smits, *Phys. Rev. Lett.* **108**, 094501 (2012).
- [3] P. Vincenti, J. Klewicki, C. Morrill-Winter, C. White, and M. Wosnik, *Exp. Fluids* **54**, 1629 (2013).
- [4] C. Willert, J. Soria, M. Stanislas, J. Klinner, O. Amili, M. Eisfelder, C. Cuvier, G. Bellani, T. Fiorini, and A. Talamelli, *J. Fluid Mech.* **826**, R5 (2017).
- [5] M. Samie, I. Marusic, N. Hutchins, M. Fu, Y. Fan, M. Hultmark, and A. Smits, *J. Fluid Mech.* **851**, 391 (2018).
- [6] M. Ono, N. Furuichi, Y. Wada, N. Kurihara, and Y. Tsuji, *Phys. Fluids* **34**, 045103 (2022).
- [7] X. Wu and P. Moin, *J. Fluid Mech.* **630**, 5 (2009).
- [8] P. Schlatter and R. Örlü, *J. Fluid Mech.* **659**, 116 (2010).
- [9] J. Jimenez, S. Hoyas, M. Simens, and Y. Mizuno, *J. Fluid Mech.* **657**, 335 (2010).
- [10] M. Lee and R. Moser, *J. Fluid Mech.* **774**, 395 (2015).
- [11] S. Pirozzoli, J. Romero, M. Fatica, R. Verzicco, and P. Orlandi, *J. Fluid Mech.* **926**, A28 (2021).
- [12] S. Hoyas, M. Oberlack, F. Alcantara-Avila, S. Kraheberger, and J. Laux, *Phys. Rev. Fluids* **7**, 014602 (2022).
- [13] J. Yao, S. Rezaeiravesh, P. Schlatter, and F. Hussain, *J. Fluid Mech.* **956**, A18 (2023).
- [14] A. Townsend, *The structure of turbulent shear flow* (Cambridge University Press, 1976).
- [15] I. Marusic, W. Baars, and N. Hutchins, *Phys. Rev. Fluids* **2**, 100502 (2017).
- [16] I. Marusic and J. Monty, *Annu. Rev. Fluid Mech.* **51**, 49 (2019).
- [17] A. Smits, *J. Fluid Mech.* **940**, A1 (2022).
- [18] X. Chen and K. R. Sreenivasan, *J. Fluid Mech.* **908**, R3 (2021).
- [19] X. Chen and K. R. Sreenivasan, *J. Fluid Mech.* **933**, A20 (2022).
- [20] X. Chen and K. R. Sreenivasan, *J. Fluid Mech.* **976**, A21 (2023).
- [21] P. Monkewitz, *J. Fluid Mech.* **931**, A18 (2022).
- [22] H. Nagib, R. Vinuesa, and S. Hoyas, *Utilizing indicator functions with computational data to confirm nature of overlap in normal turbulent stresses: logarithmic or quarter-power* (2024), 2405.14675.
- [23] C. Meneveau and I. Marusic, *J. Fluid Mech.* **719**, R1 (2013).
- [24] N. Hutchins, T. Nickels, I. Marusic, and M. Chong, *J. Fluid Mech.* **635**, 103 (2009).
- [25] P. Schlatter, Q. Li, R. Örlü, F. Hussain, and D. Henningson, *Euro. J. Mech. B/ Fluids* **48**, 75 (2014), ISSN 0997-7546, URL <https://www.sciencedirect.com/science/article/pii/S09977546>
- [26] A. Perry, S. Henbest, and M. Chong, *J. Fluid Mech.* **165**, 163 (1986).
- [27] M. Vallikivi, B. Ganapathisubramani, and A. Smits, *J. Fluid Mech.* **771**, 303 (2015).
- [28] R. Panton, M. Lee, and R. Moser, *Phys. Rev. Fluids* **2**, 094604 (2017).
- [29] M. Hultmark, M. Vallikivi, S. C. C. Bailey, and A. Smits, *J. Fluid Mech.* **728**, 376–395 (2013).
- [30] S. Diwan and J. F. Morrison, 11th International Symposium on Turbulence and Shear Flow Phenomena (TSFP11) **728**, Southampton, UK (2019).
- [31] B. Birnir, L. Angheluta, J. Kaminsky, and X. Chen, *Phys. Rev. Res.* **3**, 043054 (2021), URL <https://link.aps.org/doi/10.1103/PhysRevResearch.3.043054>.